Visible light responsive TiO_2 nanotubes synthesized by electrochemical anodization method

Elizabeta Stojcheva[1], Metka Benčina[2]*, Ita Junkar[2], Tomaž Lampe[3], Matjaz Valant[4,5], Veronika Kralj-Iglič[3], Aleš Iglič[2,6]

[1]Laboratory of Biophysics, Faculty of Electrical Engineering, University of Ljubljana, Tržaška 25, SI-1000 Ljubljana, Slovenia
[2]Jožef Stefan Institute, Department of Surface Engineering and Optoelectronics, Jamova 39, SI-1000 Ljubljana, Slovenia
[3]Laboratory of Clinical Biophysics, Faculty of Health Sciences, University of Ljubljana, Zdravstvena 5, SI-1000 Ljubljana, Slovenia
[4]Materials Research Laboratory, University of Nova Gorica, Vipavska 13, SI-5000 Nova Gorica, Slovenia
[5]Institute of Fundamental and Frontier Sciences, University of Electronic Science and Technology of China, Chengdu 610054, China
[6]Laboratory of Clinical Biophysics, Faculty of Medicine, University of Ljubljana, Zaloška 9 5, SI-1000 Ljubljana, Slovenia

*Corresponding author

DOI: 10.5185/amlett.2018.2024
www.vbripress.com/aml

Abstract

The photocatalytic activity of TiO_2 nanotubes (NTs) makes these materials promising candidates for a variety of applications, including photocatalytic degradation, water splitting and biomedical devices. The large band gap of TiO_2 (anatase ~3.2 eV; rutile ~ 3.0 eV) requires excitation with UV light, which accounts for only a small fraction of solar light. In order to increase the light absorption in the visible region, reduction of the band gap is required. Here, TiO_2 nanotubes (NTs) were fabricated by electrochemical anodization of Ti foil. Scanning electron microscopy (SEM), X-ray diffraction analysis (XRD) and X-ray photoemission spectroscopy (XPS) were used to determine morphology, crystal structure and surface composition of the TiO_2 NTs. Different synthesis conditions influenced TiO_2 NTs properties that allowed the tuning of the band gap. UV-Vis analysis of 61.54 μm long NTs showed light absorption over the whole visible range, while NTs with the length up to 0.21 μm are able to absorb only UV light. 61.54 μm long NTs exhibited band tailing up to 1.43 eV.

Keywords: TiO_2 nanotubes, electrochemical anodization, visible light absorption, band gap.

Introduction

TiO_2 nanotubes (NTs) offer attractive technological advantages in a variety of applications, such as photocatalytic water and air purification [1, 2], water photoelectrolysis [3, 4] and dye-sensitized solar cells [5, 6], due to high chemical stability, non-toxicity and corrosion resistance. Besides promising photocatalytic utilization, TiO_2 NTs are highly biocompatible materials that attracted significant interest for biomedical application. Due to unique morphology-dependent physicochemical properties such as high specific surface area, nano-roughness, highly ordered structure, surface charge and wettability, which all affect their interaction with biological materials, TiO_2 NTs have advantage before widely used metallic Ti and its alloys.

In general, native TiO_2 is photoactive only under UV light due to its wide band gap (3.0 eV and 3.2 eV for rutile and anatase, respectively) [7] and capable of absorption of only small fraction of the solar spectrum (3-5 %). In order to improve its sensitivity to visible light, various bandgap engineering approaches have been developed, involving coupling of TiO_2 with other materials (e.g. CdS quantum dots [8], plasmonic Au [9], graphene [10]) and band gap narrowing by doping with various atoms (e.g. carbon - C [11], nitogen - N [12], sulphur - S [13]), which often require two-step synthesis method. Some of the biomedical applications such as photodynamic therapy for cancer treatment [14], photo-induced drug delivery systems [15], photo/electro-chemical biosensors [16] and antibacterial surfaces [17] require the use of light energy, therefore band gap engineering of TiO_2 NT is of significant importance.

In present study, we report on the effect of NTs morphology on their optical properties. Electrochemical anodization is cost effective and simple method to produce self-organized NTs arrays with highly controllable geometry; varying synthesis parameters e.g. anodization time, applied voltage and electrolyte

composition influence the NTs length, diameter, nanopore/nanotube formation and open tops of NTs [18]. Theoretical predictions indicate that TiO_2 NTs diameter highly influences its electronic structure [19].

Although TiO_2 NTs are widely studied, there is still lack of information about their optical properties. To the best of our knowledge, a systematic investigation of the light absorbance and band gap energy of self-assembled TiO_2 NTs has not yet been reported. Here, TiO_2 NTs were produced by electrochemical anodization of Ti foil at different synthesis conditions. The effect of morphology on the light absorption is demonstrated and the mechanism of the band gap reduction is proposed.

Experimental

Materials

Titanium foil (Advent, 0.1 mm thickness, 99.6%), ethylene glycol - EG (Fluka, ≥99.5%), H_2O (miliQ), ammonium fluoride - NH_4F (Sigma Aldrich, 28.0-30.0%), ethanol (Sigma Aldrich, 96%), hydrofluoric acid - HF (Sigma Aldrich, ≥40%) and acetone (Honeywell Riedel - de Haen, 99.5%).

Material synthesis

TiO_2 NTs were fabricated with electrochemical anodization method of Ti foil. Experiments were carried out at a room temperature (≈ 20 °C) in a system with two electrodes with a working distance of 1.5 cm. The ethylene glycol based electrolytes allows for fabrication of highly ordered NTs arrays [20], while fluoride ion concentrations are responsible for formation of porous oxides, therefore in present study NH_4F and HF as a sources of fluoride ions were used. H_2O was added to the electrolyte, since allows for the transition of nanopores to nanotubes [20].

The pre-treatment was performed in order to obtain a pre-dimpled surface, which leads to higher surface homogeneity with fewer defects on the surface of the NTs grown in the second step as shown in previous studies [18, 20]. Before anodization, Ti foil was ultrasonically cleaned in acetone, ethanol and deionized (DI) water, 5 min in each and further dried under a nitrogen stream. The electrolyte used in this step was composed of ethylene glycol and 0.35 wt. % NH_4F with the addition of 1.7 wt. % H_2O and was the same for all NTs. Nanotubular layer grown in this step was then removed with successive ultrasonication in H_2O, acetone and ethanol.

In the second step of anodization process, the pretreated Ti surfaces were used as a substrate to grow NTs. The electrolyte based on an ethylene glycol, containing water and HF or NH_4F was used. Detailed synthesis parameters of this step are presented in **Table 1**. As-synthesized NTs were kept in ethanol for 2 hours in order to remove all organic components from the electrolyte and dried under a nitrogen stream. As-prepared NTs were additionally annealed at 450 °C for 1h in air atmosphere with annealing/cooling rate = 8 °C/min and as such used for further characterization.

Table 1. The effect of the synthesis conditions on the diameter, length and crystallite size of the synthesized TiO_2 NTs.

Sample	Voltage (V)	Time (h)	Electrolyte (wt. %)	Diameter (nm)	Length (μm)
NT15	10	1	HF (1.1), H_2O (15.3), EG	15	0.21
NT50	40	1	HF (1.1), H_2O (15.3), EG	50	1.26
NT100	58	2.5	HF (1.0), H_2O (11.0), EG	100	2.53
NT100-L	58	17	NH_4F (0.3), H_2O (1.8), EG	100	61.54

Characterizations

Morphology of the NTs was analyzed by scanning electron microscope (SEM - JSM 7100F - JEOL) equipped with a thermal field emission gun with an accelerating voltage of 15 kV.

X-ray diffraction (XRD) analysis was performed by MiniFlex 600 Benchtop X-ray Defractometer (Rigaku) using Cu Kα radiation. Data were collected in a range $10 \leq 2\theta \leq 70°$, with a scan step of 0.017°, divergence slit of 0.218° and counting speed 10°/min.

The X-ray photoelectron spectroscopy (XPS) analyses were carried out on the PHI-TFA XPS spectrometer produced by Physical Electronics Inc. The high-energy resolution spectra were acquired by the energy analyzer operating at resolution of approximately 0.6 eV and pass energy of 29 eV. During data processing the spectra from the surface were aligned by setting the C1s peak at 285.0 eV, characteristic for C–C bonds. The accuracy of binding energies was approximately ± 0.3 eV. Quantification of surface composition was performed from XPS peak intensities taking into account relative sensitivity factors provided by instrument manufacturer. Three different XPS measurements were performed on each sample and average composition was calculated. The XPS spectra were measured for NT100 sample immediately after the anodization and after thermal treatment. The depth profile analysis of NT100 was conducted in order to observe the changes in chemical composition in lower layers of the surface. The Ar^+ ion beam with 1 keV energy was used for sputtering at an incidence angle of 45° and a raster of 5 mm x 5 mm. The sputtering rate was approximately 1 nm/min.

Diffusive reflectance spectroscopy (DRS) was used to evaluate absorption of light and band gap energies of the materials. The samples were analysed with a PerkinElmer Lambda 650S (Waltham, MA) spectrophotometer in a 250–700 nm spectral range. A Spectralon reflection standard was used as a reference. The diffuse reflectance spectra were converted into the absorption spectra by the Kubelka-Munk equation [21]. Since it was previously shown that the anatase TiO_2 have indirect band gap [22], the band gap energies were determined by plotting $[F(R\infty)h\nu]^{1/2}$ versus $h\nu$.

Results and discussion

The electrochemical process of TiO_2 NTs formation after sufficient applied voltage can be divided into three steps: (i) formation of an oxide layer (Eq. 1), (ii) pore formation and (iii) nanopores to nanotubes transition.

$$Ti + 2H_2O \rightarrow TiO_2 + 4H^+ + 4e^- \quad (1)$$

$$TiO_2 + 6F^- + 4H^+ \rightarrow TiF_6^{2-}2H_2O \quad (2)$$

The exact process of TiO_2 NTs growth is still not known, however it is assumed that the tube elongation is governed by a competition between (i) field assisted oxidation of the Ti metal - formation of TiO_2 at metal/oxide interface and (ii) chemical dissolution at tube mouth and field-assisted dissolution of formed oxide at the tube bottom layer (oxide/electrolyte interface). According to Lockman *et al.* [23] the applied voltage controls the degree of field assisted dissolution, which causes inwards growth of NTs at the bottom part of the NTs (oxide/electrolyte interface). The effect of electrochemical and chemical etching rate determines the NTs length: if the electrochemical dissolution rate at tube bottom is faster than the chemical dissolution rate at tube mouth, the NTs grow longer [24].

Different types of NTs were formed depending on the applied voltage, concentration of electrolyte and time (as presented in Table 1). When the synthesis time was fixed at 1h in HF-containing electrolyte, 10 V of applied voltage resulted in 210 nm thick uniform layer of nanopores with around 20 nm in diameter – NT15 - **Fig. 1A**. It was previously reported that the water in the electrolyte is responsible for nanotube formation, since it acts as a source of oxygen for oxide formation and as a component which induce the separation of the nanopores at cell boundaries - "pore-wall-splitting" mechanism [25-27]. The formation of NT15 and separation of nanopores to nanotubes can be explained by one of the theoretical models, which suggests that the electric field that moves towards oxide/electrolyte interface is responsible for transport of Ti^{4+} ions towards the oxide surface, where filed-assisted dissolution takes place. Fluoride ions from the electrolyte solution react with ejected Ti^{4+} ions from the Ti metal and with formed oxide layer (TiO_2) and form water soluble complexes- $[TiF_6]^{2-}$ (Eq. 2), that are accumulated at cell boundaries. It was experimentally proven that these metal/oxide interfaces are composed of $[TiF_6]^{2-}$ species [28]. As $[TiF_6]^{2-}$ species are water soluble, the fluoride-rich layers are prone to chemical dissolution by water [26]. Despite the water and fluoride concentration in the electrolyte was the same at 10 V, 40 V and 58 V applied voltages in present study, the 10 V is not enough to initiate "pore-wall-splitting" mechanism. Regonini *et al.* [29] suggest that chemical dissolution of fluoride rich layers increases with higher voltages (> 10 V in their study), because higher electric field is responsible for weakening the Ti-O bond and favouring the chemical attack of fluoride ions. The same was shown in present study; at higher voltage (40 V) well-defined nanotubes with empty space in between were formed (**Fig. 1B**). The diameter of as formed NTs (40 V) is 50 nm, while length is 1.26 µm. With further increase in applied voltage (58 V) and time (2.5 h), NTs diameter and length increase to 100 nm and 2.53 µm, respectively – NT100 (**Fig. 1C**). Similar results were obtained before [18, 30]. According to these findings, the electrochemical dissolution prevails above chemical dissolution with increasing of the applied voltages. In order to prepare longer NTs, NH_4F^- based electrolyte was used. As the synthesis time increased to 17h, significant increase in NT100-L length (61.5 µm) was observed, while diameter was still 100 nm as for NT100 (**Fig. 1D**). SEM analysis of the annealed samples revealed that the structure of NTs remained undistorted.

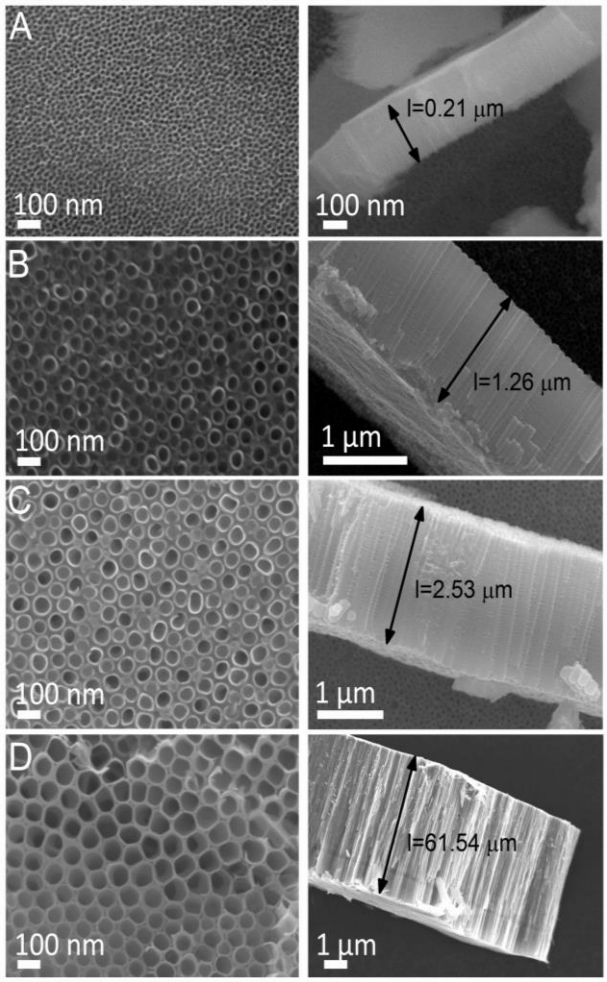

Fig. 1. The top and cross section morphology of synthesized TiO_2 NT15 - (A) and (B), TiO_2 NT50- (C) and (D), TiO_2 NT100 - (E) and (F) and TiO_2 NT100-L - (G) and (H) analyzed by SEM.

X-ray diffraction analysis revealed the amorphous nature of as-anodized TiO_2 NTs (in **Fig. 2** the sample of as-anodized NT100 is presented, while similar spectra were obtained for other NTs). After annealing at 450 °C for 1h, XRD peaks of NTs samples correspond to anatase crystal structure, as can be seen from **Fig. 2**. Small anatase peak was also observed for NT15.

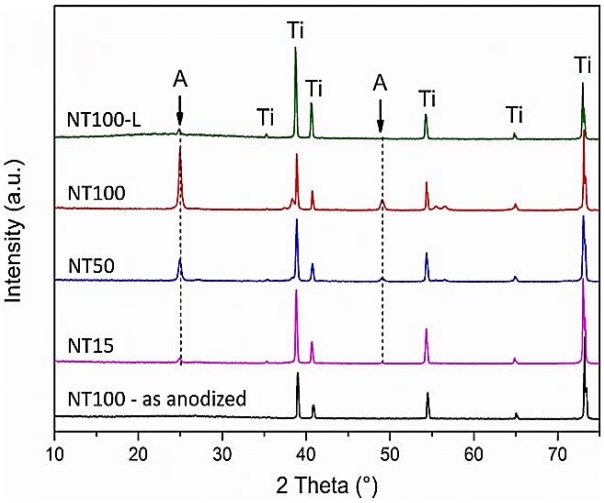

Fig. 2. XRD patterns of synthesized TiO_2 NTs; A - peaks corresponding to anatase crystal structure, Ti - peaks corresponding to Ti foil.

It has been previously reported that TiO_2 NTs prepared by electrochemical anodization method contain some electrolyte residues, in particular fluoride and carbon, despite cleaning the samples with the ethanol immediately after the synthesis [18]. The XPS analysis conducted on as-anodized NT100 and annealed NT100 confirmed the contamination with electrolyte remainings. The as-anodized NT100 sample contains fluoride on the surface, beside titanium, oxygen and carbon, (**Fig. 3A**). XPS analysis confirmed the absence of fluoride on the annealed NT100 (**Fig. 3B**).

There were no differences in the C 1s peaks for the as-anodized and annealed NTs, as seen from **Fig. 3C**. The concentration of carbon remains the same (30 at. %) even after 17-h anodization followed by annealing of NT100-L at 450°C for 1h (data not shown). These results show that by the thermal treatment carbon atoms ae not removed from the surface of NTs, while fluoride can be successfully eliminated.

Analysis of the C 1s core levels peaks showed prominent peak at 285 eV, which is indicative for adventitious carbon (C-C, C=C and/or C-H bonds). However, no characteristic peak was found at 281 eV corresponding to Ti-C, this indicates that carbon was not doped into the TiO_2 lattice as suggested in Ref. [31]. This was also confirmed by depth profile analysis, as no carbon was detected on the surface after 2 min of sputtering of the surface with Ar^+ (corresponding depth is 2 nm) (**Fig. 3D**). Thus carbon is merely present as contaminant on the top surface of TiO_2 nanotubes. The peaks at ~ 286 and ~ 289 eV correspond to C-O-C, C=O and O-C=O **(Fig. 3c)**, which means that carbon is partially oxidized on the surface, however in literature also Ti-O-C bonds can be correlated to this binding energy [31]. As mentioned Ti-C bond (281 eV) as present in pure titanium carbide was not observed, neither was detected by XRD.

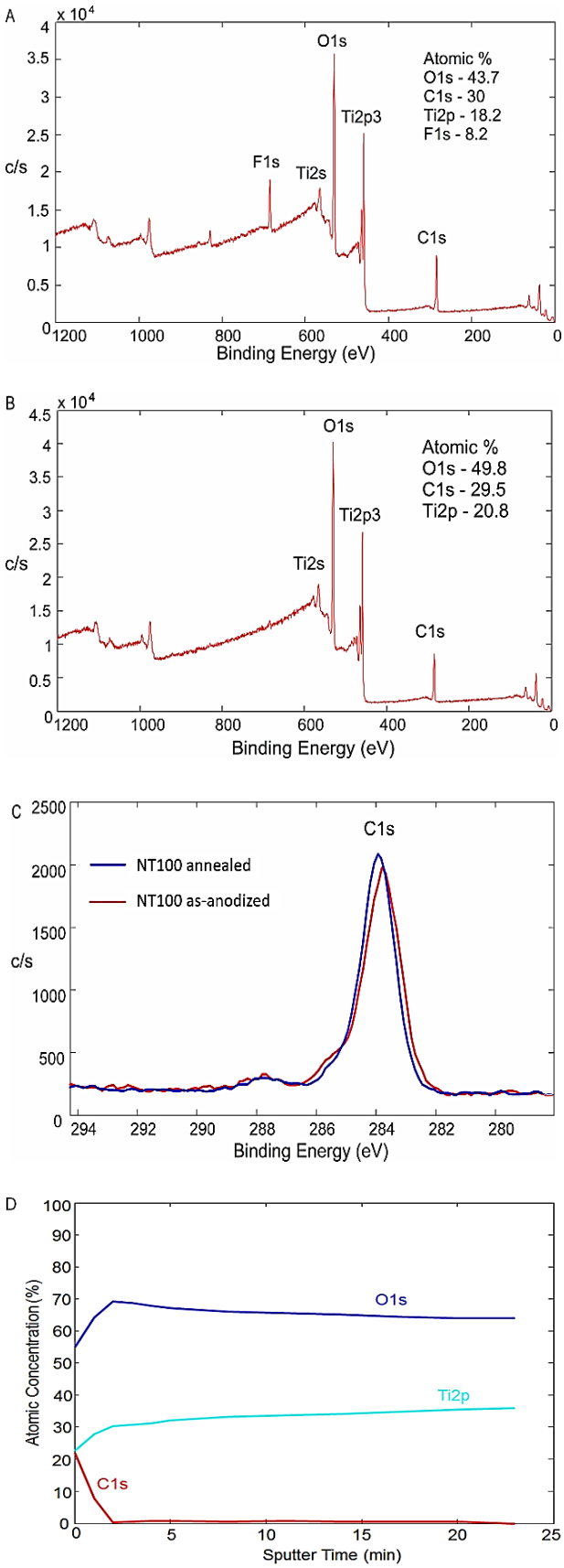

Fig. 3. XPS analysis of as-anodized (A) and annealed NT100 (B) and comparison of C 1s peaks (C) and depth profile analysis of NT100 sample (D).

UV-Vis spectroscopy analysis revealed that maximum absorption edge of NTs with length up to 2.5 µm (NT100) is at ~380 nm, therefore this samples absorb UV light (**Fig. 4A**). However, there are some differences in light absorption among annealed and as-anodized samples; the maximum absorption edge for the as-anodized NTs is slightly shifted towards longer wavelengths. Besides, it can be seen in **Fig.4A** that the maximum absorption edge is increasing with increasing NTs length. Correspondingly, the band gaps of NT15-NT100 follow the trend; the lowest band gap energy was observed for the annealed NT100-3.27eV and the widest band gap for as-anodized NT15 - 3.53eV (**Fig. 4B)**.

The color of NT100-L (length = 61.5 µm) is darker, which indicates the absorption of light of higher wavelengths as compared to shorter NTs (≤ 2.5 µm). The UV-Vis spectroscopy analysis of NT100-L is consistent with its brown-colored appearance; as-anodized and annealed NT100-L samples showed absorption over the whole visible region (400-700 nm) along with the UV light absorption (**Fig. 4C**), although the diameter of these NTs is the same (100 nm) as of the 2.5 µm long NT100. The band gap of NT100-L is reduced with respect to other samples (**Fig. 4D**). However, it is intriguing that as-anodized amorphous NT100-L sample exhibits a bandgap almost identical to crystalline.

Kurian *et al.* [32] connected the capability of visible light absorption of ~12 µm long TiO_2 NTs with 100 nm in diameter to the surface layer composed of substitutional and interstitial carbon atoms, which are the consequence of the annealing process in air atmosphere. Carbon atoms introduce a structural disorder and localized states at the surface along with oxygen vacancies, which effectively reduces the band gap and allows the visible light absorption. Shorter time of annealing (30 min at 450 °C) in Ref. [32] resulted in high carbon content and visible light absorption of ~12 µm long TiO_2 NTs, while for 3 h annealed sample at 450 °C, carbon in the samples was not observed by XPS analysis and the maximum absorption edge of TiO_2 NTs was in the UV region [32]. It is well known that carbon can induce visible light absorption of TiO_2; band gap narrowing occurs due to the overlap of the O 2p and dopant states [33].

The band gap analysis by DRS of the NT100-L indicates the band tailing; initial band gap of the annealed and as-anodized NT100-L is 3.00 eV and 3.05 eV with the surface band gap of 1.53 eV and 1.43 eV, respectively. Kurian *et al.* [32] attribute the band tailing nature of NTs to the surface carbon content. Authors propose band model with bulk band gap of 3.32 eV and surface band gap of 1.7 eV [32], similar as in present study. The XPS spectra of NT100 synthesized in the present study confirmed the presence of carbon at the surface of as-anodized as well as annealed (1h at 450 °C) samples; 30 at. % and 29.5 at. % of carbon, respectively. The XPS analysis also confirmed carbon atoms in the annealed NT100-L sample (30 at. % - data not shown). Similar carbon content on the surface of the as-anodized and annealed NT100 and annealed NT100-L indicates that carbon cannot be the reason for better NT100-L visible light absorption performance, moreover it has been shown that carbon is merely present on the top surface layer of NTs (about 2 nm in depth).

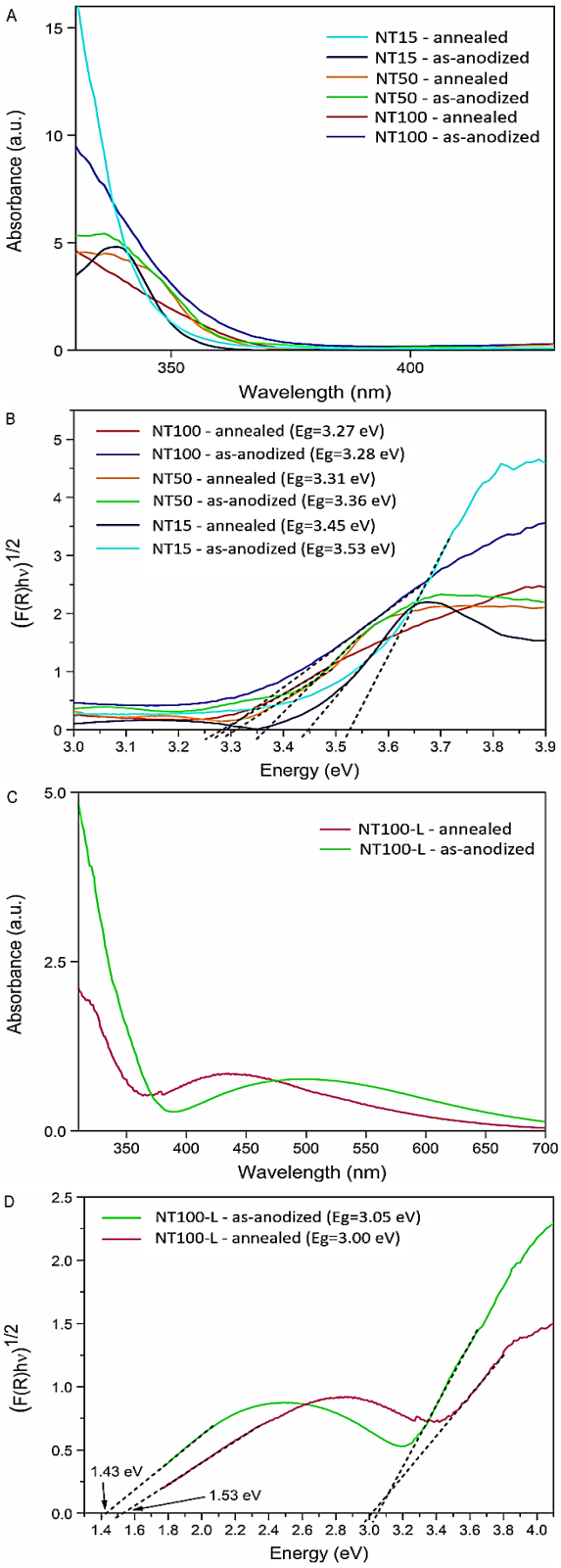

Fig. 4. UV-visible absorbance spectra of as-anodized and annealed NTs (A, C) and the corresponding band gap energies of indirect electron transition calculated by the Kubelka–Munk function (B, D).

However, the main difference in surface chemical composition between as-anodized and annealed NTs synthesized in the present study is in the content of fluoride. The XPS results of the annealed NT100 do not show its characteristic peak at 484 eV, while as-anodized sample contains 8.2 at. % of the fluoride. It was reported that the presence of fluoride in the lattice induces the formation of reduced Ti^{3+} centers that localize the extra electron needed for charge compensation [34]. Yu *et al.* [35] claim that the crystallinity of anatase TiO_2 was improved upon fluoride doping and samples exhibited stronger absorption in the UV-visible range with a red shift in the band gap transition. In the present study, all NTs samples, as-anodized and annealed, showed similar light absorbance characteristics. Besides, similar concentrations of fluoride atoms in the annealed NT100 and NT100-L indicate that fluoride is not responsible for the NT100-L red shift of absorbance spectra.

Although the Ti^{3+} surface states can act as recombination centers for photogenerated charge, these states together with corresponding oxygen vacancies, can also be responsible for visible light absorption in Ti-oxides due to the formation of the band gap electronic states and its reduction [35]. Kurian *et al.* [32] stated that Ti^{3+} surface states are physically equivalent to oxygen vacancies, as a physical origin for the high visible light absorption. It was previously reported that the surface area of NTs increases with increasing length [30], therefore we suspect that higher surface area of longer NT100-L enables to generate more Ti^{3+} states at the surface of NTs walls, but Ti^{3+} states formation cannot be due to the presence of fluoride or carbon atoms at the surface of the NTs.

Formation of Ti^{3+} states commonly requires post-anodizing treatments [36], annealing in a controlled atmosphere [37], air plasma treatment [38], etc.. Introduction of the Ti^{3+} states into NTs crystal structure by a simple method is therefore challenging. Results of this study show that the 17-h electrochemical anodization method enables production of visible light sensitive NTs. It has been demonstrated that NT100-L band gap reduction is not chemically induced, but is probably related to physical changes in the material during electrochemical anodization. Assumingly, longer time (17h) exposure of NT100-L to anodization conditions, is responsible for the formation of surface defects/oxygen vacancies/Ti^{3+} states that significantly reduce NT100-L band gap energy.

Conclusions

The increase of the applied voltage leads to increase of the TiO_2 NTs diameter and length up to 61.5 μm - NT100-L. Apparently, higher voltage induces higher electric field that drives field assisted dissolution (elongation of TiO_2 NTs) and chemical dissolution - splitting of pores to nanotubes. The length of NTs plays significant role in the band gap narrowing and visible light absorption. NTs with length up to 2.5 μm (NT100) absorb only UV light, while 61.5 μm long NT100-L are visible light sensitive. Assumingly, the reason for visible light absorption and band tailing of NT100-L is higher Ti^{3+} surface states content on the larger surface area of the as-anodized and annealed NT100-L, which induces reduction in the band gap. The narrower band gap of shorter NT50 and NT100 is 3.27 eV (amorphous NT100), while annealed NT100-L has bulk band gap of 3.00 eV and surface band gap of 1.53 eV. In present study it was demonstrated that NTs, capable of efficient visible light absorption, can be synthesized with an electrochemical anodization method.

Acknowledgements

This work was supported by Slovenian Ministry of Education, Science and Sport grant "Public call for encouraging young investigators at the beginning of their career 2.0", No.5442-15/2016/18 and by the Slovene Research Agency grants No. P2-0232 and J2-8166.

References

1. Liu, Z.; Zhang, X.; Nishimoto, S.; Murakami, T.; Fujishima, A.; *Environ. Sci. Technol.*, **2008**, *42*, 8547-8551. **DOI:** 10.1021/es8016842
2. Quan, X.; Ruan, X.; Zhao, H.; Chen, S.; Zhao, Y.; *Environ. Pollut.*, **2007**, *147*, 409-414. **DOI:** 10.1016/j.envpol.2006.05.023
3. Mohapatra, S. K.; Misra, M.; Mahajan, V. K.; Raja, K. S.; *J. Phys. Chem. C.*, **2007**, *111*, 8677-8685. **DOI:** 10.1021/jp071906v
4. Park, J. H.; Kim, S.; Bard, A. J.; *Nano Lett*., **2006**, *6*, 24-28. **DOI:** 10.1021/nl051807y
5. Shankar, K.; Mor, G. K.; Prakasam, H. E.; Yoriya, S.; Paulose, M.; Varghese, O. K.; Grimes, C. A.; *Nanotechnology*, **2007**, *18*, 065707. **DOI:** 10.1088/0957-4484/18/6/065707
6. Zhu, K.; Neale, N. R.; Miedaner, A.; Frank, A. J.; *Nano Lett.*, **2007**, *7*, 69-74. **DOI:** 10.1021/nl062000o
7. Tang, H.; Prasad, K.; Sanjines, R.; Schmid, P.; Levy, F.; *J. Appl. Phys.*, **1994**, *75*, 2042-2047. **DOI:** 10.1063/1.356306
8. Li, G.-S.; Zhang, D.-Q.; Yu, J. C.; *Environ. Sci. Technol.*, **2009**, *43*, 7079-7085. **DOI:** 10.1021/es9011993
9. Zhang, Z.; Zhang, L.; Hedhili, M. N.; Zhang, H.; Wang, P.; *Nano Lett.*, **2012**, *13*, 14-20. **DOI:** 10.1021/nl3029202
10. Liang, Y.; Wang, H.; Casalongue, H. S.; Chen, Z.; Dai, H.; *Nano Res.*, **2010**, *3*, 701-705. **DOI:** 10.1007/s12274-010-0033-5
11. Irie, H.; Watanabe, Y.; Hashimoto, K.; *Chem. Lett*., **2003**, *32*, 772-773. **DOI:** 10.1246/cl.2003.772
12. Morikawa, T.; Asahi, R.; Ohwaki, T.; Aoki, K.; Taga, Y.; *Jpn. J. Appl. Phys.*, **2001**, *40*, 561. **DOI:** 10.1143/JJAP.40.L561
13. Umebayashi, T.; Yamaki, T.; Itoh, H.; Asai, K.; *Appl. Phys. Lett.*, **2002**, *81*, 454-456. **DOI:** 10.1063/1.1493647
14. Lee, C.; Hong, C.; Kim, H.; Kang, J.; Zheng, H. M.; *J. Photochem. Photobiol.*, **2010**, *86*, 981-989. **DOI:** 10.1111/j.1751-1097.2010.00731.x
15. Kim, D.; Macak, J. M.; Schimidt-Stein, F.; Schmuki, P.; *Nanotechnology*, **2008**, *19*, 305710. **DOI:** 10.1088/0957-4484/19/30/305710
16. Huo, K.; Gao, B.; Fu, J.; Zhao, L.; Chu, P. K.; *RSC Adv*, **2014**, *4*, 17300-17324. **DOI:** 10.1039/C4RA01458H
17. Akhavan, O.; Abdolahad, M.; Abdi, Y.; Mohajerzadeh, S.; *Carbon*, **2009**, *47*, 3280-3287. **DOI:** 10.1016/j.carbon.2009.07.046

18. Kulkarni, M.; Mazare, A.; Schmuki, P.; Iglic, A.; *Adv. Mat. Lett.*, **2016**, *7*, 23-28.
DOI: 10.5185/amlett.2016.6156
19. Liu, Z.; Zhang, Q.; Qin, L.-C.; *Solid State Commun*., **2007**, *141*, 168-171.
DOI: 10.1016/j.ssc.2006.09.055
20. Roy, P.; Berger, S.; Schmuki, P.; *Angew. Chem. Int. Ed*., **2011**, *50*, 2904-2939.
DOI: 10.1002/anie.201001374
21. Morales, A. E.; Mora, E. S.; Pal, U. Rev. Mex. Fis., **2007**, *53*, 18-22.
DOI: 10.3390/ijms12031496
22. Zhang, J.; Zhou, P.; Liu, J.; Yu, J.; *Phys. Chem. Chem. Phys*., **2014**, *16*, 20382-20386.
DOI: 10.1039/c4cp02201g
23. Lockman, Z.; Sreekantan, S.; Ismail, S.; Schmidt-Mende, L.; MacManus-Driscoll, J. L.; *J Alloys Compd*., **2010**, *503*, 359-364.
DOI: 10.1016/j.jallcom.2009.12.093
24. Gong, D.; Grimes, C. A.; Varghese, O. K.; Hu, W.; Singh, R.; Chen, Z.; Dickey, E. C.; *J. Mater. Res*., **2001**, *16*, 3331-3334.
DOI: 10.1557/JMR.2001.0457
25. Wei, W.; Berger, S.; Hauser, C.; Meyer, K.; Yang, M.; Schmuki, P.; *Electrochem commun*., **2010**, *12*, 1184-1186.
DOI: 10.1016/j.elecom.2010.06.014
26. Riboni, F.; Nguyen, N. T.; So, S.; Schmuki, P.; *Nanoscale Horiz*., **2016**, *1*, 445-466.
DOI: 10.1039/C6NH00054A
27. Kulkarni, M.; Mazare, A.; Gongadze, E.; Perutkova, Š.; Kralj-Iglič, V.; Milošev, I.; Schmuki, P.; Iglič, A.; Mozetič, M.; *Nanotechnology*, **2015**, *26*, 062002.
DOI: 10.1088/0957-4484/26/6/062002
28. Berger, S.; Albu, S. P.; Schmidt-Stein, F.; Hildebrand, H.; Schmuki, P.; Hammond, J. S.; Paul, D. F.; Reichlmaier, S.; *Surf. Sci*., **2011**, *605*, 57-60.
DOI: 10.1016/j.susc.2011.06.019
29. Regonini, D.; Satka, A.; Jaroenworaluck, A.; Allsopp, D. W.; Bowen, C. R.; Stevens, R.; *Electrochim. Acta*., **2012**, *74*, 244-253.
DOI: 10.1016/j.electacta.2012.04.076
30. Kulkarni, M.; Flašker, A.; Lokar, M.; Mrak-Poljšak, K.; Mazare, A.; Artenjak, A.; Čučnik, S.; Kralj, S.; Velikonja, A.; Schmuki, P.; *Int. J. Nanomedicine*., **2015**, *10*, 1359.
DOI: 10.2147/IJN.S77492
31. Ren, W.; Ai, Z.; Jia, F.; Zhang, L.; Fan, X.; Zou, Z.; *Appl. Catal., B.*, **2007**, *69*, 138-144.
DOI: 10.1016/j.apcatb.2006.06.015
32. Kurian, S.; Seo, H.; Jeon, H.; *J. Phys. Chem. C.*, **2013**, *117*, 16811-16819.
DOI: 10.1021/jp405207e
33. Wang, H.; Lewis, J. P.; *J. Phys. Condens. Matter*., **2005**, *17*, L209.
DOI: 10.1088/0953-8984/17/21/L01
34. Czoska, A.; Livraghi, S.; Chiesa, M.; Giamello, E.; Agnoli, S.; Granozzi, G.; Finazzi, E.; Valentin, C. D.; Pacchioni, G.; *J. Phys. Chem. C.*, **2008**, *112*, 8951-8956.
DOI: 10.1021/jp8004184
35. Yu, J. C.; Yu, J.; Ho, W.; Jiang, Z.; Zhang, L.; *Chem. Mat*., **2002**, *14*, 3808-3816.
DOI: 10.1021/cm020027c
36. Xing, M.; Zhang, J.; Chen, F.; Tian, B.; *Chem. Comm*., **2011**, *47*, 4947-4949.
DOI: 10.1039/c1cc10537j
37. Liu, N.; Paramasivam, I.; Yang, M.; Schmuki, P.; *J. Solid. State. Electrochem*., **2012**, *16*, 3499-3504.
DOI: 10.1021/es0702723
38. Bharti, B.; Kumar, S.; Lee, H.-N.; Kumar, R.; *Sci. Rep*., **2016**, *6*.
DOI: 10.1038/srep3235

